An Estimated Shape Function for Drift in a Platelet-Transport Model

Chinjung Yeh, Anne C. Calvez, and Eugene C. Eckstein
Departments of Biomedical Engineering, University of Miami, Coral Gables, Florida 33124 and University of Tennessee, Memphis, Tennessee 38163 USA

ABSTRACT Prior work has shown that concentration profiles of platelets in flowing whole blood and of platelet-sized beads in flowing blood suspensions can include near-wall excesses. A model to describe this phenomenon was built about a single-component convective diffusion equation. To incorporate redistribution to preferred sites by shear flows of red cell suspensions, the model used a drift shape function (in addition to the commonly used augmented diffusion coefficient). This paper reports experiments that provide an average concentration profile from which the shape function for that model is calculated; the experiments and shape function are for the particular conditions of 40% hematocrit, platelet-sized latex beads (2.5 μm diameter), tube ID of 217 μm, and a wall shear rate of 555 s^{-1}. Less precise estimates of the shape function obtained from data of previous studies indicate that the shape function is similar for the hematocrit of 15%.

INTRODUCTION

Several studies have shown that flowing blood suspensions can have concentration profiles of platelets or platelet-sized latex beads with concentrations near the wall that are three to eight times those in the central region (Tangelder et al., 1982; Tilles and Eckstein, 1987; Aarts et al., 1988; Eckstein et al. 1989; Waters and Eckstein, 1990; Koleski and Eckstein, 1991). For platelet-sized latex beads, such excesses occur when the wall shear rate is >200 s^{-1} and the hematocrit is >10% (Tilles and Eckstein, 1987). Since latex beads lack the biological responses of platelets, it is reasonable to attribute the phenomenon to physical (rheological) events.

The principle of mass action, which relates reaction rates to the concentrations of the participating species, provides a basis for expecting that near-wall excesses are important in thrombosis and other interactions among the endothelial cells, platelets, and biochemicals of the vascular system. For example, the reactive state of a platelet may depend upon how many times and how long it has been adjacent to the vascular surface, which produces substances that passivate or activate platelets. A similar rationale is appropriate for modeling damage to and interactions with platelets as blood flow carries them past biomaterials. Any description of such interactive events requires detailed information about the platelet history. With a well-defined drift function, the model discussed below can be used for both conventional field calculations and for simulations. Such computations will allow further studies of the transport and reaction processes in flowing blood.

As a part of modeling the concentration profiles observed for latex beads (platelets) in red cell suspensions (blood), Eckstein and Belgacem (1991) adapted the traditional convective diffusion equation by adding a drift term. All directed events that act to develop the near-wall peaks in the concentration profile were subsumed and described by the drift term. The adapted transport model was shown in two equivalent forms: as a traditional partial differential equation with a form similar to that used for continuum mass transfer and as a stochastic differential equation (SDE), which is well suited for simulating the motion of individual particles. Both forms use the same drift function. Particle motion described through the SDE can be readily visualized because the complex total motion can be separated into idealized motions: an individual bead or platelet experiences convection, diffusion and drift. Using an assumed mathematical form for the drift function and an enhanced diffusion coefficient of 1.25×10^{-7} cm^2/s, numerical experiments were performed to show that solutions of the mathematical equations exhibited near-wall peaks of excess concentration similar to those observed in experimental trials (Eckstein and Belgacem, 1991). Experiments reported here were used to estimate the shape of the drift function for flow of 40% hematocrit suspension through a 217-μm tube at a wall shear rate of 555 s^{-1}; a smoothed numerical approximation to the data was obtained for use in computations.

The model and shape function are *ad hoc* ways of describing events in tube flows of multicomponent suspensions, like blood. The need to specify particular conditions of tube diameter, hematocrit, and wall shear rate signals an obvious limit of the model; much effort is required for a quantitative prediction of values of the drift shape function for any particular case. This deficiency is mitigated by the fact that the drift shape function appears to be qualitatively similar for many conditions; evidence for this is discussed below.

Received for publication 28 February 1994 and in final form 20 June 1994.

Address reprint requests to Eugene C. Eckstein, University of Tennessee, Memphis, Department of Biomedical Engineering, 899 Madison Avenue, Suite 801, Memphis, TN 38163. Tel.: 901–448–7536; Fax: 901–448–7387; E-mail: eckstein@bme.utmem.edu.

0006-3495/94/09/1252/08 $2.00

MATERIALS AND METHODS

For reasons described more fully in Eckstein and Belgacem (1991), experimental parameters were selected to obtain time-invariant, fully developed concentration profiles in steady tube flows. The drift shape function was estimated through numerical calculations that used the average profile.

The experimental methods and data reduction protocol used to obtain the concentration profiles closely paralleled those used for studies of lateral transport in a transient situation (Yeh and Eckstein, 1994); accordingly, only a brief summary follows.

Suspensions of freshly washed human red cells and fluorescent 2.5- μm latex beads were made and placed in a stirred reservoir; suspension composition was fixed at 40% hematocrit with a bead count between 1.5 and $2.2 \times 10^5/\text{mm}^3$. For each trial, a syringe pump drew red cell suspension from the reservoir into and through a thin-walled polyethylene tube. A 30-min period of steady flow allowed the distribution of beads in the tube to reach steady state. Flow rates were set with the goal of having similar values of the equivalent Poiseuille wall shear rate for the set of trials; the average wall shear rate for the set was $555\ \text{s}^{-1}$. Then liquid nitrogen was poured over the tube to rapidly freeze it and its contents; this step captured the locations of fluorescent platelet-sized latex beads. Centimeter-long segments of the frozen tube located 30, 40, and 50 cm from the entrance were collected. Later, each segment was placed in a cryomicrotome on a fluorescence microscope and sectioned while frozen. After each thin layer of tube was removed, the freshly exposed remaining surface of the tube segment was viewed end-on and a digital image of the surface was recorded. This process was repeated as often as possible for each tube segment. The distances from the beads to the wall were measured on the recorded images and consolidated into a list for each segment. Using a nonparametric kernel-estimate method for estimating the probability density and a relationship between radial probability density and concentration, a radial concentration profile was obtained for each tube segment. Following the equations shown in Waters and Eckstein (1990), the concentration values in each profile were normalized with respect to the reservoir concentration.

Several limits of the experimental methods are fundamental to understanding and interpreting the data. The numerical aperture of the objective used to collect images (0.75) is a primary limit on resolution of distances. Common estimates for transmitted light microscopy indicate that two edges located 1.5 μm apart can be resolved with this objective; blooming and other events of fluorescence microscopy, which are difficult to estimate, slightly lessen the resolution; these were minimized by using the minimum level of illumination for effective image collection. Based on apparent image size, calibration of distances with a stage micrometer, and the supplier's size for the latex beads, we estimate the maximum error associated with blooming to be ~0.5 μm. Sampling frequency for digital image collection was at more than twice the optical resolution, and thus not a concern. Particle positions were calculated as being at the centroid of the region of bright pixels. The wall was located as the apparent edge traced in the image. The processes of spotting particles and drawing the wall were done independently. When the lists of wall coordinates and particle centers were fed into the program that calculated the least distance between each particle and the wall, the program occasionally reported the non-physical (impossible) outcome of a particle-to-wall distance that was less than the particle radius. Such values were attributed to the limited ability to resolve edges and centers; they were not changed.

The kernel-estimate process for calculating the probability density, which leads to the concentration profile, involved a choice that related to the accuracy of resolving the radial position of individual particles. In the kernel estimate, a probability density distribution was placed at each place a particle was sighted. To find the overall probability density, these individual contributions for each particle were summed and normalized. Use of a symmetric triangular probability distribution for each particle was computationally convenient. The base of the triangle was chosen to be equal to the diameter of the bead, a size which approximated the total uncertainty in the optical measurement of the radial position. Since the triangular distribution can be viewed as a weighting of the possible locations where each particle could have been found, the kernel-estimate process was consistent with the experimental accuracy. For similar reasons, an absolute criterion was built into the density estimate program to deal with sightings near the wall; no individual triangle of probability density was allowed to extend beyond the wall. Considering the overall kernel-estimate process shows that, as a set, the data were judged to be relatively precise (meaning that the proportion of measurements near a particular off-wall location was essentially correct, i.e., within statistical limits for the number of particles sighted) but not especially accurate (meaning that the absolute value of the off-wall position of individual particles could be incorrect). Comparison of kernel estimates with histograms constructed directly from the lists of distance measurements showed that all major features of the profile were maintained; the major virtue of the kernel estimate was its smoothness, which leads to less "noise" in estimating the derivative of the concentration profile.

Two measures of the concentration profiles, defined in earlier studies (Eckstein et al., 1989), were used to characterize the near-wall peaks in the profiles. One measure was the height of the near-wall peak; the other was the distance from the wall to the first point on the central side of the peak where the normalized concentration equaled one plus half the excess concentration at the peak. These measures, peak height and peak extent, were used in statistical tests performed using SigmaStat software (Jandel, Inc., San Rafael, CA).

The Results section describes a rationale, based on a statistical test, for considering each concentration profile to be an equal representative of a parent populace. For an individual tube segment, the output from the kernel-estimate program is in the form of concentration values that are uniformly spaced in the radial direction. An average concentration profile was obtained by averaging the concentration values for all trials for each off-wall position. These averages were computed using the distance from the wall to avoid any "smearing" of the profile in the near-wall zone. Since the tubes had slightly different radii, such smearing would occur if the calculations were done with respect to the center of the tube or if they were done with respect to a normalized radial coordinate. Last, it should be noted that the process for estimating the peak height was conservative; when each observation of a particle was equally weighted, the average concentration profile had a 15% greater amplitude of near-wall excess than the one shown here. However, the location of the peak was the same for both curves.

Equation for the drift shape function

Eckstein and Belgacem (1991) show that the drift function can be estimated from the balance of lateral events (diffusion and the drift) in the region where the concentration profile is fully developed, i.e, the axial location where there is no longer any change of velocity or concentration profiles. To summarize those concepts, the flux in the radial direction at such locations, J_r, can be expressed in terms of the fully developed, steady-state concentration, c_{fd}, and ordinary derivatives (because there is no axial or tangential variation) by

$$J_r = V_{drift} c_{fd} - D \frac{dc_{fd}}{dr}. \quad (1)$$

Here, V_{drift} is a drift velocity; D, an enhanced diffusion coefficient; and r, the radial coordinate in the tube. The term $V_{drift}\, c_{fd}$ represents that part of the flux due to drifting (directed) motion in the radial direction. The right-most term is the classical Fickian expression that represents flux caused by a concentration gradient; D provides a measure of the apparent diffusive (random) motion. The flux, J_r, is 0 at the wall; by use of a control volume and the principle of mass conservation, it is readily shown to be 0 at all other radial positions. Assuming that c_{fd} is not 0 at any radial location and that the diffusion coefficient does not depend on time or position, the expression for V_{drift} follows directly by algebraic manipulation; it is

$$V_{drift} = \frac{D}{c_{fd}} \frac{dc_{fd}}{dr}. \quad (2)$$

(*Note:* In some models where the value of D varies in space, the drift velocity can include a term associated with the variation of D; for situations in which the drift is the primary cause of local excess accumulations, this correction is small. This topic will be treated more extensively in a future publication.) Use of the definition of the derivative of the logarithm provides a second form of the expression, i.e.,

$$V_{drift} = D \frac{d(\ln c_{fd})}{dr}. \quad (3)$$

Dividing the drift function by the diffusion coefficient, which for physical

reasons is always not 0, yields an expression that depends only on the fully developed concentration profile; this expression, which is referred to as the drift shape function, is

$$\frac{V_{drift}}{D} = \frac{1}{c_{fd}} \frac{dc_{fd}}{dr} = \frac{d(\ln c_{fd})}{dr}. \quad (4)$$

Note that the scale of V_{drift} depends upon the diffusion coefficient and that only the shape function for the drift is estimated here.

Numerical approximations of the expressions for Eq. 4 were used to estimate the drift shape function. Direct translations of the two forms of Eq. 4 into finite difference numerical approximations (Press et al., 1992) were computed first and considered as unbiased estimates. A 0.5-μm step size was used in the numerical approximations. Reflecting our belief that the drift function will be a relatively smooth function, the Savitsky-Golay (S-G) method of filtering was chosen to obtain an estimate with less ripple; S-G methods were developed to estimate peak locations and are relatively robust for estimating the local slope (Press et al., 1992). In a conventional S-G filter, a number of equally spaced points is chosen on both sides of each point where a smoothed estimate is desired. Typically that number of points is between one to two times the number of points that fall across the half-height of the peak that is being characterized. The points on both sides and the center point are used to compute a least-squares fit for a low-order power-law function through the center point. Fitting of the power law with redundant information provides a local smoothing of the curve. This process is repeated at each point in the region where the filter is applied. Power-law functions are useful in expressions like the equations, since they are readily converted to derivatives.

Near the wall the S-G method cannot be applied directly since there are no meaningful points on the far side of the wall. This problem was avoided by writing a PV-Wave program (Visual Numerics, Sugarland, TX) that followed the general principle for S-G filters. For the calculated point nearest the wall, the program used the five points in the concentration profile closest to the wall (two on either side of the point and the point itself). For the next point, the number of points was increased by two (so that there were three points on either side of the point). The number of points was increased by two for each subsequent point further into the tube until 13 points on either side were used. A fourth degree polynomial was used for the first point and sixth degree for all other points.

Even after S-G filtering, the drift changed sign in some portions in the central region, which, if carried blindly into the model, would predict small peaks in the concentration profile in the central region of the tube. Such features were treated as errors and attributed to the noisy process of numerical differentiation and the limited accuracy of the data. Hence, a further modification was made: the region from 16.76 μm to the center was fitted with an exponential decay curve that passed through the drift values as estimated at the last two points before the exponential decay curve (at 15.76 and 16.26 μm). This led to a value of drift in the center that is ~0, which is expected because of symmetry.

RESULTS

Five trials were run using the steady state protocol with a suspension hematocrit of 40%, an average tube ID of 217 μm, and a wall shear rate of 555 s^{-1}; three tube segments were collected from each trial. The numbers of cross-sectional images and of wall-bead distance measurements are listed in Table 1; there were greatly different numbers of cross-sectional surfaces for different segments because, even after much practice, images with strong contrast and clearly demarcated objects were difficult to obtain. Concentration profiles were estimated for each segment; to provide a tangible understanding of the variation of the data, profiles for all segments appear in Fig. 1. The peak heights and peak extents for the concentration profiles provided one summary of these trials; these data are also shown in Table 1. Inspection of those values shows that while the peak height varied both among trials and for segments cut at various distances along the tube, the peak extent varied much less. This finding paralleled past studies (Waters and Eckstein, 1990; Koleski and Eckstein, 1991).

All of the particle-wall distance measurements were amalgamated into a list, which was sorted into 1-μm-wide bins to demonstrate the relative distribution of bead-to-wall distances independently of the process of estimating concentration profiles. The resulting histogram reaffirmed the off-wall location of the peak. The bins for the intervals from 2 to 3 μm and from 3 to 4 μm had statistically indistinguishable counts (1253 and 1236, respectively). Also, the counts in these bins were significantly higher than those for the adjacent intervals (the bin from 1 to 2 μm had 1005 counts and the bin from 4 to 5 μm had 987 counts). If the peak were at the wall, the bin from 1 to 2 μm would have the largest counts. This observation is consistent with prior work

TABLE 1 Parameters and values

Tube/segment ID	Diameter (μm)	Wall shear rate (s^{-1})	No. of sections	No. of beads	Peak height	Peak extent (μm)
SA-30	227	492	25	1068	12.6	5.3
SA-40	222	525	18	749	12.1	4.5
SA-50	228	483	19	835	11.6	5.3
SB-30	211	584	32	1113	7.5	6.7
SB-40	221	507	34	1303	8.9	5.7
SB-50	207	612	14	348	11.2	5.5
SD-30	229	571	32	1333	7.0	6.9
SD-40	208	771	33	1198	6.1	7.7
SD-50	238	511	21	802	7.3	5.5
SE-30	210	524	16	597	10.6	5.1
SE-40	216	484	20	727	4.4	9.8
SE-50	206	562	27	935	5.7	8.0
SF-30	214	542	27	861	6.3	6.1
SF-40	212	557	36	1251	7.5	6.2
SF-50	208	595	30	1151	7.6	5.8
Mean	217	555			8.4	6.3
SD	9.5	70			2.5	1.3

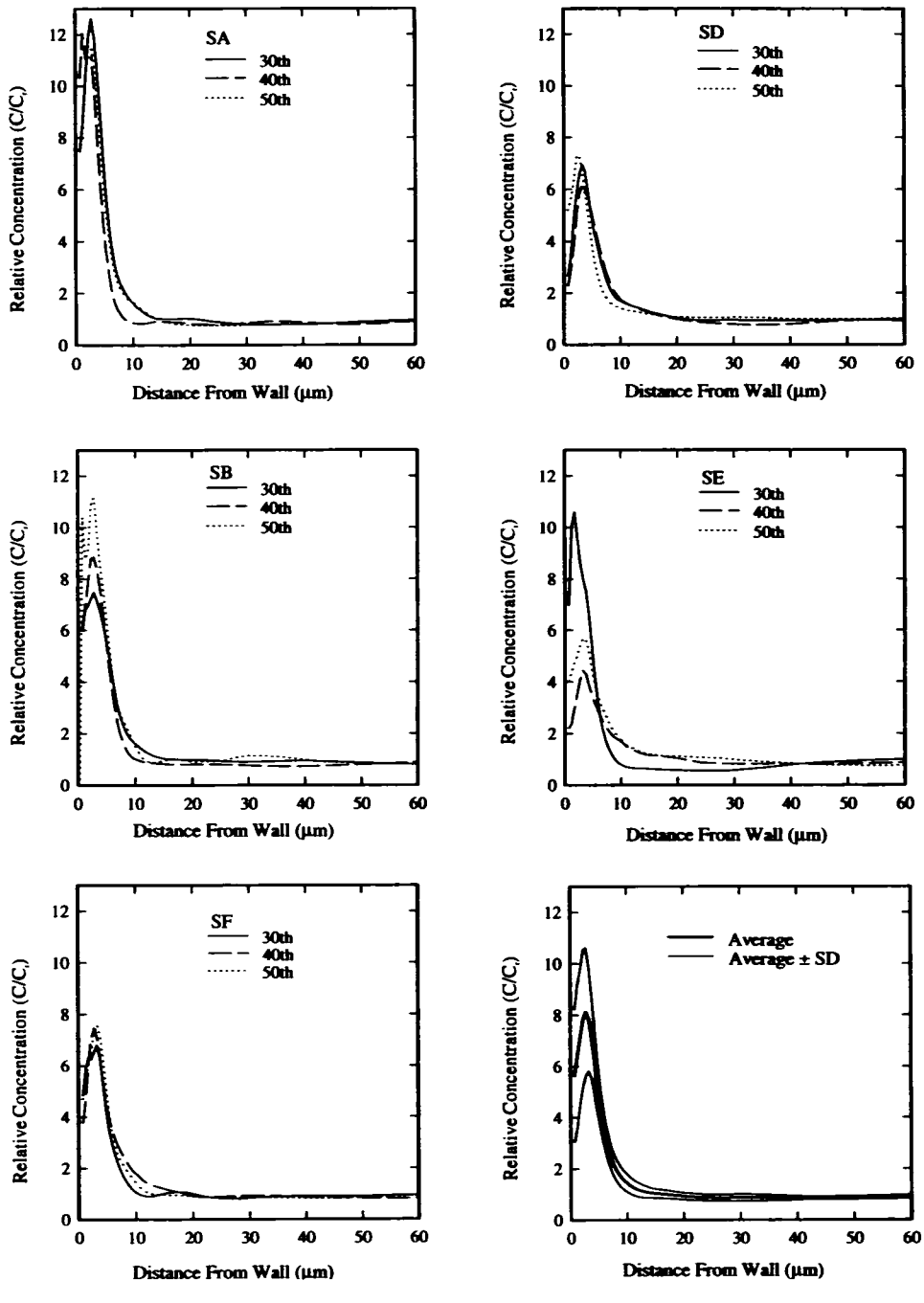

FIGURE 1 Concentration profiles from individual segments of the five tubes and the average concentration profile with error bands (*bottom right corner*). See text for further information.

showing that the peak is slightly off the wall (Waters and Eckstein, 1990; Tilles and Eckstein, 1987).

Statistical testing, via a two-way analysis of variance with a balanced design, used the null hypothesis that there was no difference in the value of a feature at the various axial locations where segment were collected; tube/trial identity was used as the second factor. The features of the concentration profiles that were tested were the peak height, peak width, and product of peak height and peak width. No significant difference with respect to axial location was found for any of the three features; p values for the various measures tested ranged from 0.49 to 0.85. The lack of statistical difference was taken as an indication that the profiles were representative samples of an underlying, much larger populace that describes either an ideal concentration profile or an underlying complex process from which individual realizations can be observed. Our rationale for the latter viewpoint appears below.

To estimate the underlying populace, a segment-based average was calculated from the 15 individual concentration profiles; it is shown in the lower right corner panel of Fig. 1. The standard deviation of the concentration at the radial positions provides a measure of the range of profiles that might be drawn from the ideal population. The lighter lines in the last panel of Fig. 1 correspond to the average value ± SD. A smaller number, the SEM, provides an indication of the

relative confidence for estimating the mean concentration profile. If bands showing the mean ± SEM were drawn about the average profile, they would be 26% of the width of the SD bands.

Drift shape function

Both forms of Eq. 4 were used to numerically estimate the shape function from the average fully developed concentration profile. When plotted on the same graph, the two estimates of the shape function overlapped and were visually indistinguishable. In addition, a numerical calculation based on the cumulative probability density was tried; that calculation produced a very noisy estimate of the drift, which possessed the gross features of the other estimates. In retrospect, such an outcome might be expected since the calculation involving the cumulative density used a ratio of second and first numerical derivatives.

The shape of an average drift function as directly calculated with finite difference versions of the equations is shown in the upper panel of Fig. 2. Shown as dashed lines on either side of the drift shape function are estimates of the propagation of error from the mean concentration profile. The SEM was used in the propagation of error calculations since the estimates of the drift based on the equations involved the mean value of the concentration at each point. By elementary calculus, the 0 of the drift shape function corresponds to the peak of the near-wall excess. This estimate of peak position is consistent with the value obtained by binning the observations, an occurrence which suggests that numerical differentiation did not greatly degrade the estimated shape function. The "off-wall" nature of the excess is reflected in the sign change of the shape of the drift. Particles located in the few micrometers nearest the wall drift away from the wall; the remainder drift toward the wall. Note that substantial drift occurs over a region larger than the obvious peak; the region extends to about 25 μm from the wall. Little drift occurs in the central, major portion of the tube.

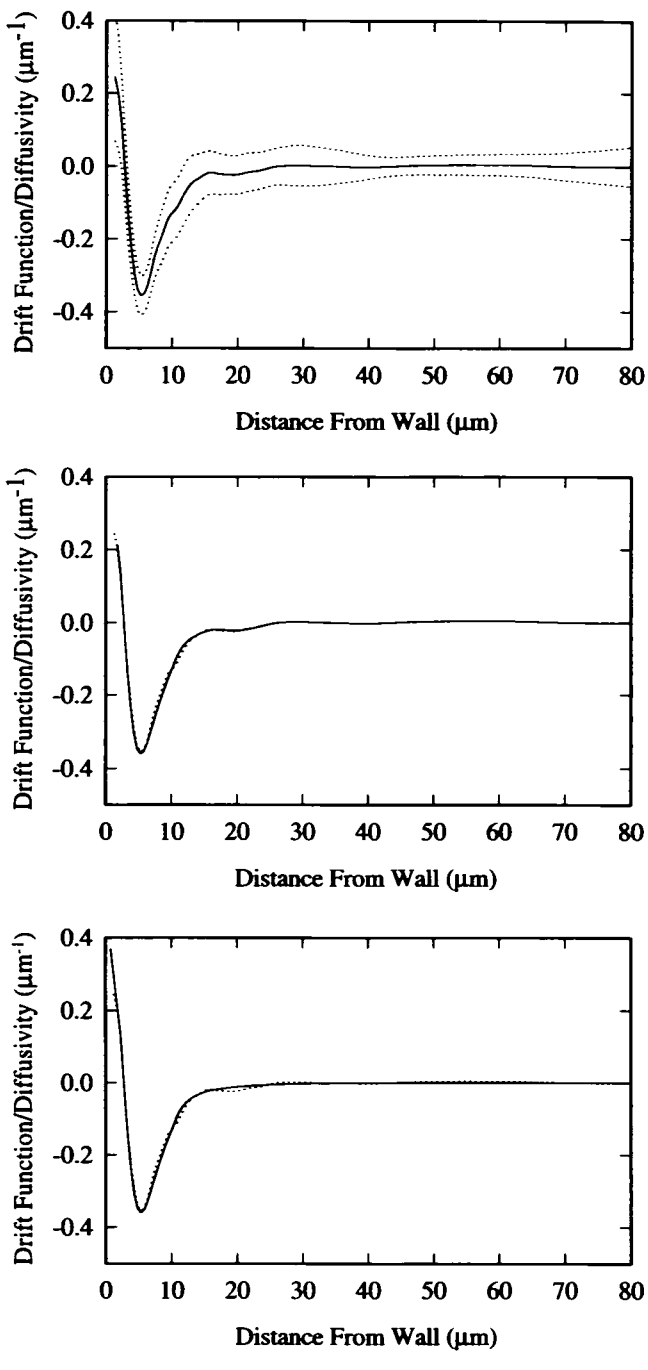

FIGURE 2 Estimated drift shape functions for 40% hematocrit, 2.5 μm beads, 217 μm tube ID, and wall shear rate of 555 s^{-1}. (*Top*) Solid line depicts the finite-difference numerical estimate (FDNE) of the drift shape function; the dashed lines provide error bands showing the propagation of error in the calculation. (*Center*) Solid line depicts the S-G smoothed estimate; the dashed line is the FDNE of the upper panel. (*Bottom*) Solid line shows the S-G curve with an exponential decay fitted for the central portion; the dashed line is the FDNE for comparison.

DISCUSSION

The great variation of the peak height that appears in the data set (see Fig. 1) naturally provokes questions. Is there a single ideal concentration profile with the variation among profiles shown in Fig. 1 fundamentally related to the quality of the measurements or are the individual profiles realizations of a more complex random process that is intrinsic to the redistribution phenomenon? The practical difficulties connected with the experiments add legitimacy to the first question. An inspection of Table 1 shows that there is variation of diameter along the tube, which unavoidably leads to a variation of wall shear rate. By design the minimum shear rate for the tests is well above the value where onset of large near-wall excesses occurs; that shear rate is ~400 s^{-1}. Statistical test of peak height (see the data in Table 1) indicates no significant variation with the wall shear rate or the local diameter. Another possible cause involves miscounting the beads in the images. Locating beads in an image requires contrast, which is reduced when there are many beads, because those below the region of focus lead to background haze in the images. If this were a problem, the lower peaks shown in the data set might be due to a systematic undercounting for cases of low contrast. However, a review of the data, e.g., by considering the

TABLE 2 Estimated and smoothed values

R-r	Numerical	S-G drift	Final drift	*R-r*	Numerical	S-G drift	Final drift
0.76			0.3684	26.26	0.00005389	−0.0008279	−0.004492
1.26	0.2442		0.2899	26.76	0.000685	0.0002196	−0.004167
1.76	0.2026	0.2115	0.2115	27.26	0.001108	0.00101756	−0.003865
2.26	0.1198	0.1331	0.1331	27.76	0.001438	0.001576	−0.003584
2.76	−0.006143	−0.003748	−0.003748	28.26	0.001705	0.001926	−0.003324
3.26	−0.1289	−0.12903	−0.1290	28.76	0.001926	0.002107	−0.003083
3.76	−0.2221	−0.2310	−0.2310	29.26	0.002085	0.002136	−0.002860
4.26	−0.2935	−0.3036	−0.3035	29.76	0.002137	0.002025	−0.002653
4.76	−0.3401	−0.3464	−0.3464	30.26	0.001897	0.001790	−0.002460
5.26	−0.3562	−0.3599	−0.3599	30.76	0.001445	0.001466	−0.002282
5.76	−0.3498	−0.3532	−0.3532	31.26	0.000741	0.001102	−0.002116
6.26	−0.3280	−0.3324	−0.3324	31.76	0.0001604	0.0007359	−0.001963
6.76	−0.2918	−0.3042	−0.3042	32.26	−0.0002139	0.0003985	−0.001821
7.26	−0.2516	−0.2744	−0.2744	32.76	−0.0004202	0.0001047	−0.001689
7.76	−0.2220	−0.2451	−0.2451	33.26	−0.0004356	−0.0001500	−0.001566
8.26	−0.1987	−0.2166	−0.2166	33.76	−0.0004357	−0.0003849	−0.001453
8.76	−0.1728	−0.1897	−0.1897	34.26	−0.0005046	−0.0006144	−0.001347
9.26	−0.1482	−0.1646	−0.1646	34.76	−0.0004894	−0.0008446	−0.001250
9.76	−0.1329	−0.1412	−0.1412	35.26	−0.0005966	−0.001071	−0.001159
10.26	−0.1239	−0.1195	−0.1195	35.76	−0.0007575	−0.001286	−0.001075
10.76	−0.1123	−0.09581	−0.09581	36.26	−0.0009492	−0.001486	−0.0009971
11.26	−0.09555	−0.07751	−0.07751	36.76	−0.001402	−0.001665	−0.0009248
11.76	−0.07785	−0.06416	−0.06416	37.26	−0.001840	−0.001823	−0.0008578
12.26	−0.06225	−0.05424	−0.05424	37.76	−0.002102	−0.001957	−0.0007956
12.76	−0.05001	−0.04651	−0.04651	38.26	−0.002297	−0.002067	−0.0007379
13.26	−0.04177	−0.04044	−0.04044	38.76	−0.002523	−0.002148	−0.0006844
13.76	−0.03627	−0.03545	−0.03545	39.26	−0.00251	−0.002195	−0.0006348
14.26	−0.03082	−0.03111	−0.03111	39.76	−0.002344	−0.002195	−0.0005887
14.76	−0.02463	−0.02737	−0.02737	40.26	−0.002184	−0.002138	−0.0005461
15.26	−0.01941	−0.02425	−0.02425	40.76	−0.002017	−0.002011	−0.0005065
15.76	−0.01733	−0.02182	−0.02182	41.26	−0.001787	−0.001810	−0.0004698
16.26	−0.01862	−0.02024	−0.02024	41.76	−0.001471	−0.001541	−0.0004357
16.76	−0.02085	−0.01957	−0.01877	42.26	−0.001146	−0.001211	−0.0004041
17.26	−0.02225	−0.01956	−0.01741	42.76	−0.0007905	−0.0008360	−0.0003748
17.76	−0.02295	−0.01997	−0.01615	43.26	−0.0004109	−0.0004295	−0.0003476
18.26	−0.02337	−0.02064	−0.01498	43.76	−0.000007753	−0.000008274	−0.0003224
18.76	−0.02402	−0.02144	−0.01389	44.26	0.0003954	0.0004132	−0.0002991
19.26	−0.02451	−0.02202	−0.01288	44.76	0.0008215	0.0008209	−0.0002774
19.76	−0.02408	−0.02213	−0.01195	45.26	0.001239	0.001206	−0.0002573
20.26	−0.02242	−0.02167	−0.01108	45.76	0.001587	0.001560	−0.0002386
20.76	−0.01983	−0.02076	−0.01028	46.26	0.001926	0.001883	−0.0002213
21.26	−0.01767	−0.01947	−0.009535	46.76	0.002248	0.002174	−0.0002053
21.76	−0.01621	−0.01788	−0.008844	47.26	0.002539	0.002433	−0.0001904
22.26	−0.01494	−0.01603	−0.008203	47.76	0.002782	0.002662	−0.0001766
22.76	−0.01377	−0.01397	−0.007608	48.26	0.002962	0.002864	−0.0001638
23.26	−0.01246	−0.01175	−0.007056	48.76	0.003081	0.003044	−0.0001519
23.76	−0.01047	−0.009483	−0.006545	49.26	0.003183	0.003198	−0.0001409
24.26	−0.00782	−0.007315	−0.00607	49.76	0.003255	0.003334	−0.0001307
24.76	−0.005035	−0.005348	−0.00563	50.26	0.003311	0.003454	−0.0001212
25.26	−0.002684	−0.003619	−0.005222	50.76	0.003397	0.003561	−0.0001124
25.76	−0.001070	−0.002113	−0.004843	51.26	0.003513	0.003653	−0.0001043

The exponential decay curve is given by $-\exp(a[R - r] + b)$ with $a = -0.1505$ and $b = -1.4525$. For the right-hand column, values for points at and beyond 16.76 μm are calculated from the decay curve. The two points nearest the wall in the right-hand column are calculated by linear extrapolation from the S-G fitted curve.

number of beads found per cross-section, shows that the number hovers close to the average for almost all segments. Further, some of the largest peaks are found when there are the largest numbers of beads per cross-section, a situation where it is very likely that there are many haze-contributing beads below the focal region. Other aspects of the experimental method were considered, and while some led to improvements in experimental technique that are being applied to ongoing studies, no reason was found to believe that the major part of the variation among the profiles is due to error.

Definitive statements about the variation of profile features are difficult to justify, but we believe that the variation is much more likely to be a natural aspect of the event. From a mathematical perspective, variation of peak heights is to be expected if the basic phenomenon is characterized by a probability distribution that is broad and skewed, as opposed to Gaussian and narrow. Consider that the peak height represents a complex conditional probabilistic event composed of many individual random processes: each profile occurs because beads released uniformly across the entrance at a variety of times move under the influence of the suspension flow to a range of radial locations at a downstream station, where they are captured by the freezing process; in doing so, these beads provide a representation of the steady probability

distribution (average profile) for all beads entering the tube. A review of scales associated with analytically tractable conditional Markov processes, e.g., times for processes to exit an interval or to reach a particular point, shows that the means and standard deviations for these events are often of the same size (Gillespie, 1992). Compared to such events, our data have a relatively small amount of variation (see the means and standard deviations in Table 1).

Turbulence, to which the mixing process in blood has been compared, provides two vantage points for viewing the variation of peak heights among trials. First, it is well known that turbulence in tube flows exhibits great irregularity in its strength at various locations along the tube axis; dye injection studies, from O. Reynolds onward, have shown that some axial locations are strongly mixed while others are approximately laminar in their behavior (Landahl and Mollo-Christensen, 1992). Being dynamic, events at a given axial location change with time. In our case, the freeze-capture process locks in the events at the time of freezing. Various combinations of profiles with small and large peak heights could occur in the same tube flow, and possibly, the low peaks occur in regions that are less well mixed. Second, our method of data reduction parallels the method of ensemble averages, a technique that is commonly used for turbulence. Data from a number of experiments are agglomerated to find a single estimate of a statistical property describing the underlying process. Following this viewpoint, each experimental trial is a realization of a complex random process; the range of variation among the realizations is an indication of the complexity of the physical phenomenon; only the general behavior is shared among the individual trials.

Another reason to believe the physical phenomenon is intrinsically complex is that the process involves dispersion rather than molecular diffusion. Cussler, in an excellent book on diffusion (1984), chose to devote a separate chapter to dispersion processes, which by definition, involve both concentration differences and fluid flow. He noted that although dispersion and diffusion are mathematically similar, care must be taken when examining dispersive phenomena because their process dynamics cannot be predicted from diffusion alone. The redistribution phenomenon may be more complex than the many textbook cases of dispersion, since it originates in flows of concentrated suspensions (instead of continuum fluids). This aspect is crucial: the sizes of features in the profile are at the lower limit for which continuum models of the suspension are reasonable (consider, e.g., the width of the peak and the red cell diameter). Ensemble methods are often the only way to estimate the properties in such situations.

Reasons for filtering the drift shape curve

The "fine details" of the estimated drift shape curve are likely to be artifacts connected with the particular sample of experimental data and the numerical processing. Intuitively, it seems that the drift shape function should be smooth. Following this concept, the modified S-G filtering technique

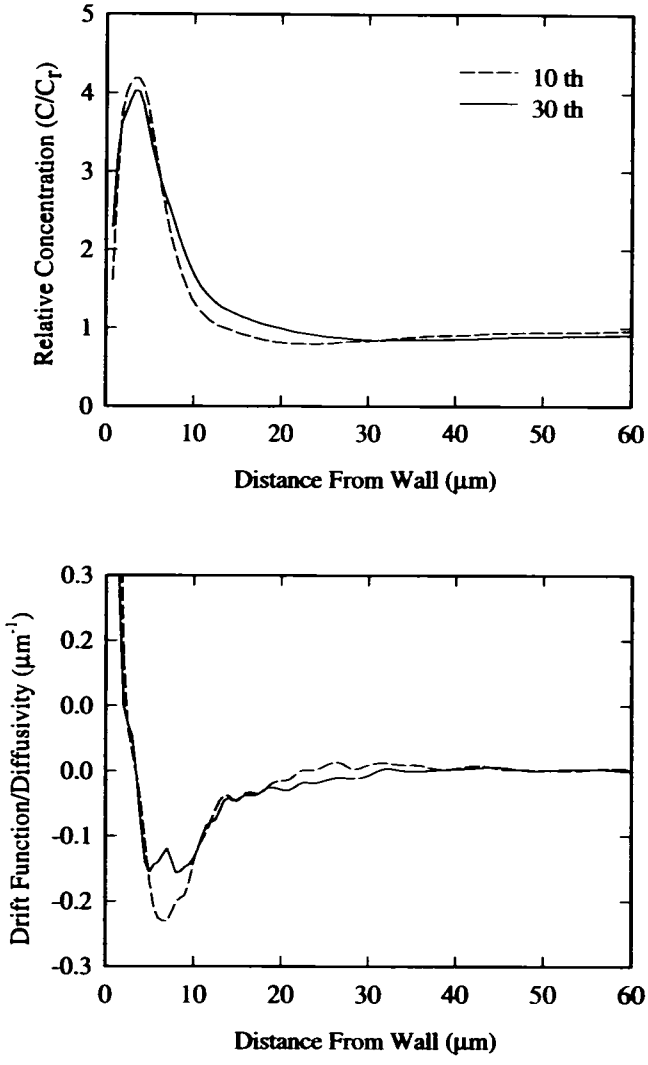

FIGURE 3 Concentration profiles for tube flow of suspensions of 15% hematocrit (*top*) and estimates of the drift shape function (*bottom*). Data taken from Waters (1987).

was used to smooth the shape function; the filtered shape function is shown as the solid line in central panel of Fig. 2. The S-G filter smooths well and follows the basic data in the region of the dip, but is not sufficient to remove all the unexpected minor features in the region from about 20 μm off the wall to the center. To smooth the central region, an exponential decay curve was fit from the last points that appeared to be well fit through the S-G process. The combined result of S-G smoothing and a fitted exponential decay is shown as the solid curve in the bottom panel of Fig. 2. A listing of the estimated values and the smoothed values at various off-wall locations (R-r) appears in Table 2. Using the stochastic equations shown in Eckstein and Belgacem (1991), the value of the diffusion coefficient noted there, and the smoothed drift shape function with the exponential decay, simulations of transient experiments (Yeh and Eckstein, 1994; Yeh, 1991) yield profiles that resemble the experimentally measured profiles. Further computer simulations are being done as a part of estimating the diffusion coefficient.

An experimental demonstration of the shape function with a smooth decay to 0 at the center may be difficult for several reasons. Obviously, the number, accuracy, and consistency of the experimental data, factors discussed above, are important. The degree to which the profile is fully developed is both crucial and difficult to ascertain. Numerical computations with the extended model showed that the middle of the tube is the last region to develop during the formation of the near-wall excess during flow into a tube (Eckstein and Belgacem, 1991). Blind use of the equations to estimate the drift shape function from partially developed calculated profiles, such as appear in Fig. 5 of (Eckstein and Belgacem, 1991) or the published experiments (e.g., Waters and Eckstein, 1990), would produce a drift shape function with a central region having a centrally directed drift. Consideration of the calculated profiles and the theory indicates that the magnitude of the true shape function would be larger than one estimated from partially developed concentration profiles. The logarithmic transformation that is a part of the definition of the drift (see equations) lessens the difference from what might be expected by visual inspection of concentration profiles. Importantly, the numerical experiments shown in Eckstein and Belgacem (1991) demonstrate that the radial position of the peak changes very little over the region of axial development, thus implying that estimates of the drift shape function from less than fully developed concentration profiles will correctly indicate key features.

It is well worth remembering that a simple model is being applied to a complex situation. Just as there is redistribution of platelet-sized particles due to the flow, there is almost certainly some redistribution of red cells. An assumption built into the model is that the events giving rise to the drift are unchanged in the axial direction (Eckstein and Belgacem, 1991); among other things, this assumption implies that the red cell distribution remains axially invariant. Most persons knowledgeable in the area of microvascular rheology would agree that some lateral redistribution of red cells toward the center of the tube does occur and will lead to increased values of red cell concentration in the center of the tube at locations further from the entrance. Such red cell redistribution would probably facilitate the axial development of the peaks in concentration profiles of platelet-sized particles. Future experiments will attempt to show the scale of the red cell redistribution.

Other estimates of the drift function

Data previously obtained by Waters and Eckstein (1990) were used to obtain an indication of the generality of the drift shape function; the profiles were for axial locations 10 and 30 cm from the entrance, for suspensions of 15% hematocrit, for shear rates of 700 s^{-1} and 900 s^{-1}, and for tubes of ~200 μm ID. The estimated shape functions were more irregular than that shown in Fig. 2; this was attributed to the smaller numbers of data in the two sets. These estimates and the profiles from which they originated are shown in Fig. 3; they have the same general shape as that in Fig. 2, but have lesser amplitude (an ~30% reduction) and a slightly greater off-wall distance over which the drift has significant influence. These general features are consistent with the lesser amount of lateral transport and the slightly broader peaks observed in the trials with suspensions of lower hematocrit.

The similarity of shape functions for the two hematocrits prompted a search for analytical functions that fit the drift shape function curves. Since the shape function resembled the attraction-repulsion curves depicted in texts on atomic physics, these were examined extensively. However, attempts to find a simple representation for either the fully developed concentration profile or the drift shape function were fruitless; the wall region of the estimated drift shape function rose less sharply than the attraction-repulsion curves.

We thank Dr. Elizabeth Tolley for advice on the statistical tests and the referees for thought-provoking critiques that helped improve the paper. This work was funded by grant HL33100 from the National Heart, Lung and Blood Institute.

REFERENCES

Aarts, P. A. M. M., S. A. T. van den Broek, G. W. Prins, G. D. C. Kuiken, J. J. Sixma, and R. M. Heethcar. 1988. Blood platelets are concentrated near the wall and red blood cells, in the center of flowing blood. *Arteriosclerosis.* 8:819–824.

Cussler, E. L. 1984. Diffusion, Mass Transfer in Fluid Systems. Cambridge University Press, New York.

Eckstein, E. C., and F. Belgacem. 1991. Model of platelet transport in flowing blood with drift and diffusion terms. *Biophys. J.* 60:53–69.

Eckstein, E. C., J. F. Koleski, and C. M. Waters. 1989. Concentration profiles of 1 and 2.5 μm beads during blood flow: Hematocrit effects. *Trans. Am. Soc. Artif. Intern. Organs.* 35:188–190.

Gillespie, D. T. 1992. Markov Processes. Academic Press, San Diego, CA.

Koleski, J. F., and E. C. Eckstein. 1991. Near-wall concentration profiles of 1.0 and 2.5 micron beads during flow of blood suspensions. *Trans. Am. Soc. Artif. Intern. Organs.* 37:9–12.

Landahl, M. T., and E. Mollo-Christensen. 1992. Turbulence and Random Processes in Fluid Mechanics, Ed. 2. Cambridge University Press, New York.

Press, W. A., S. A. Teukolsky, W. T. Vetterling, and B. P. Flannery. 1992. Numerical Recipes in C, Ed. 2. Cambridge University Press, New York.

Tangelder, G. J., D. W. Slaaf, H. C. Teirlinck, R. Alewijnse, and R. S. Reneman. 1982. Localization within a thin optical section of fluorescent blood platelets flowing in a microvessel. *Microvasc. Res.* 23:214–230.

Tilles, A. W., and E. C. Eckstein. 1987. The near-wall excess of platelet-sized particles in blood flow: its dependence on hematocrit and wall shear rate. *Microvasc. Res.* 33:211–223.

Waters, C. M. 1987. Concentration profiles of platelet-sized latex beads in blood suspensions flowing through capillary tubes. M. S. Thesis, University of Miami. Coral Gables, FL.

Waters, C. M., and E. C. Eckstein. 1990. Concentration profiles of platelet-sized latex beads for conditions relevant to hollow-fiber hemodialyzers. *Artif. Organs.* 14:7–13.

Yeh C. 1991. Direct demonstration of a radial drift of platelet-sized latex beads in flows of blood suspension. M. S. Thesis, Library, University of Miami, Coral Gables, FL.

Yeh. C., and E. C. Eckstein. 1994. Transient lateral transport of platelet-sized particles in flowing blood suspensions. *Biophys. J.* 66:1706–1716.